Ytterbium-Doped Silica Fiber Lasers: Versatile Sources for the 1–1.2 μm Region

H. M. Pask, Robert J. Carman, David C. Hanna, Anne C. Tropper, Colin J. Mackechnie, Paul R. Barber, and Judith M. Dawes

Invited Paper

***Abstract*— Ytterbium-doped silica fibers exhibit very broad absorption and emission bands, from ~800 nm to ~1064 nm for absorption and ~970 nm to ~1200 nm for emission. The simplicity of the level structure provides freedom from unwanted processes such as excited state absorption, multiphonon nonradiative decay, and concentration quenching. These fiber lasers therefore offer a very efficient and convenient means of wavelength conversion from a wide variety of pump lasers, including AlGaAs and InGaAs diodes and Nd:YAG lasers. Efficient operation with narrow linewidth at any wavelength in the emission range can be conveniently achieved using fiber gratings. A wide range of application for these sources can be anticipated. In this paper, the capabilities of this versatile source are reviewed. Analytical procedures and numerical data are presented to enable design choices to be made for the wide range of operating conditions.**

I. Introduction

AFTER the first report in 1962 of laser action in Yb^{3+}-doped silicate glass [1], Yb^{3+} has, until recently, attracted relatively little interest as a laser-active ion. It has been overshadowed by the Nd^{3+} ion with its important advantage of a four level transition, whereas Yb^{3+} has only three level and quasi-three level transitions. In fact, the most important role of the Yb^{3+} ion has so far been as a sensitizer ion, absorbing pump photons over a wide spectral range and then transferring the excitation to an acceptor ion, such as Er^{3+}, which then acts as the laser-active ion [2], [3].

More recently, interest has been shown in Yb^{3+} as a laser ion, in the form of Yb^{3+}-doped silica and fluoride fiber lasers [4]–[8], and Yb^{3+}-doped YAG [9], [10]. There are several reasons for this growth of interest. As shown in Fig. 1(a), the Yb^{3+} energy level structure is a simple one, consisting of two manifolds; the ground manifold $^2F_{7/2}$ (with four Stark levels labeled (a)–(d) in the figure) and a well-separated excited manifold $^2F_{5/2}$ (with three Stark levels labeled (e)–(g) in the figure), ~10 000 cm^{-1} above the ground level. Thus there is no excited state absorption at either pump or laser wavelengths. The large energy gap between $^2F_{5/2}$ and $^2F_{7/2}$ precludes nonradiative decay via multiphonon emission from $^2F_{5/2}$, even in a host of high phonon energy such as silica, and also precludes concentration quenching. These features contribute to the high efficiency of operation that can be achieved in Yb^{3+} lasers, as does the closeness of the pump and laser wavelengths. In fact, this energy defect, which leads to heating of the host, is a factor of ~3 smaller for Yb:YAG compared to Nd:YAG (pumped at 800 nm and lasing at 1064 nm). This reduced thermal burden is a motivating interest for Yb:YAG. Finally, the Yb^{3+} spectrum is rather broad both in absorption and emission, and particularly so in a germanosilicate host, as shown in Fig. 1(b). The broad absorption spectrum allows a wide choice of pump wavelengths. In the form of a fiber, which allows even very weak absorption to be exploited, pumping can extend from 800 nm out to 1064 nm. Similarly, for a fiber, laser operation can be made to extend well into the weak wings of the emission, provided sufficient frequency discrimination can be introduced to suppress lasing at the peaks of the emission profile. The impressive progress in development of fiber gratings [11] has made this matter of frequency discrimination very straightforward and practical, so one can now contemplate the prospect of narrow linewidth operation at any discrete wavelength between ~975 and ~1200 nm, with some degree of tunability (~1)% available by stretching or temperature tuning the grating. This range covers a number of wavelengths needed for specific applications, and these can now be generated very conveniently from an Yb^{3+}-doped silica fiber equipped with appropriate gratings. Examples include 1020 nm for pumping 1300-nm fiber amplifiers [12] and upconversion lasers based on Pr^{3+}-doped ZBLAN [13]–[15], 1140 nm for pumping Tm^{3+}-doped ZBLAN upconversion lasers [16], [17], and 1083 nm for optical pumping of He [18].

Given the wide range of different operating characteristics that might be required for various applications, and the variety of ways (e.g., different pump wavelengths) that could be used to achieve these characteristics, there is a need for a comprehensive discussion of the capabilities of Yb^{3+} fiber lasers, giving quantitative design procedures. Such has been the aim of this paper. A general discussion of Yb laser characteristics is presented in Section II. In Section III, analytical procedures and numerical data are presented to enable design choices to be made. Such calculations depend heavily on the availability of accurate absorption and emission cross section data, and the relevant spectroscopy is described in Section IV.

Manuscript received August 5, 1994; revised October 10, 1994. This work was supported by the Science and Engineering Research Council (SERC) and by the RACE II GAIN program.

H. M. Pask, D. C. Hanna A. C. Tropper, C. J. Mackechnie, P. R. Barber, and J. M. Dawes are with the Optoelectronics Research Centre, University of Southampton, HANTS SO17 1BJ, U.K.

R. J. Carman is with the Centre for Lasers and Applications, Macquarie University, N.S.W. 2109, Australia.

IEEE Log Number 9409720.

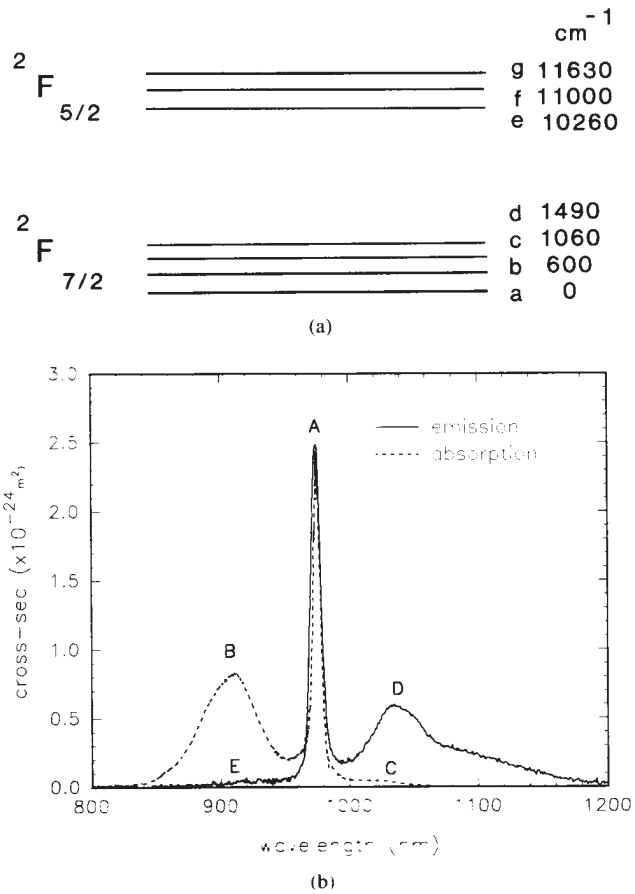

Fig. 1. (a) The Yb^{3+} energy level structure, consisting of two manifolds, the ground manifold $^2F_{7/2}$ (with four Stark levels, labeled (a)–(d)), and a well separated excited manifold $^2F_{5/2}$ (with three Stark levels labeled (e)–(g)). Approximate energies in wavenumbers above ground energy are indicated. (b) Absorption and emission cross sections for a germanosilicate host. The principal features of the spectra have been labeled A–E, and are discussed in the text.

In Sections V–VIII, some specific examples are drawn from both experimental and modeling studies of Yb^{3+}-doped silica laser action both to illustrate the agreement between modeling and experiment, and to illustrate the versatility and potential of this laser system.

II. General Discussion

The most obvious features of the absorption and emission spectra in Fig. 1(b) have been labeled (A)–(E). The narrow line at 975 nm (A) in both absorption and emission, corresponds to transitions between the lowest Stark levels in each manifold. The absorption peak at shorter wavelengths (B) corresponds to transitions from level a to f and g, while the long wavelength shoulder in the absorption spectrum (C) corresponds to transitions from level b. The weakness of this shoulder is a consequence of the much smaller population of this level (~6% of level a at room temperature, as calculated from the Boltzmann factor). Despite the weakness of this shoulder, it plays a significant role. First, it provides the means loss, having a significant effect on threshold for lasing at wavelengths within the dip in the emission spectrum.

Laser action on the narrow peak at 975 nm (A), where emission is into the lowest Stark level, is truly three-level in character. The second peak in the emission spectrum (D), with its tail extending out to 1200 nm, corresponds to transitions from level e to b, c, and d. Laser action on these transitions becomes nearly four level in character at longer wavelengths, as the emission is into essentially empty levels c and d. Transitions from level f are also evident (E), although very weak due to the small thermal population of the level, and laser action has not been observed on transitions from that level.

In general, when generation of a particular laser emission wavelength is required, there is a wide choice of possible pump wavelengths ranging from ~800 to ~1064 nm, and therefore, a choice of pump laser sources including AlGaAs and InGaAs diodes, Titanium sapphire lasers, Nd:YLF lasers and Nd:YAG lasers. As will be demonstrated in subsequent sections, extremely efficient laser action can be achieved using any of these sources. There are, however, several considerations other than the availability of sources that can go into the choice. First, one can only generate gain and hence lasing at longer wavelengths than the pump, so for example, 1020-nm operation cannot be achieved with a 1064-nm pump, but can with 975 nm pumping into the sharp absorption line. Second, pumping at 975-nm accesses the largest absorption cross section, so this is particularly appropriate where the shortest fiber length is required as for example in a single frequency laser. It is also appropriate for cladding-pumping, enabling the fiber length to be kept down to reasonable values, since the cladding-pumping geometry involves a scaling up of the absorption length, as described in Section VII. When pumping at 975 nm, it may be important to consider the effects of amplified spontaneous emission (ASE), as discussed below. Third, the slope efficiency with respect to absorbed pump power of Yb^{3+} lasers is usually dominated by the ratio of laser to pump photon energies. It is therefore possible to significantly enhance the conversion efficiency (e.g., by up to ~20% for laser action at 1140nm) by pumping close to the laser wavelength (e.g., with a Nd:YLF or Nd:YAG laser). Fourth, the pump power requirements are a function of the absorption and emission cross sections at the pump wavelength.

The critical pump power P_{cr} required to achieve a gain coefficient of zero at a particular point in the fiber (i.e., to reach transparency for the signal/laser wavelength), is given by

$$P_{cr} = \frac{Ah\nu_p}{\tau} \frac{1}{\left(\frac{\sigma_{el}\sigma_{ap}}{\sigma_{al}} - \sigma_{ep}\right)}.$$

Here we have assumed no background loss in the fiber. This expression can be readily derived from (2)–(5) in the next section, when the gain coefficient, $g(z)$, is set equal to zero and the pump quantum efficiency is assumed to equal unity.

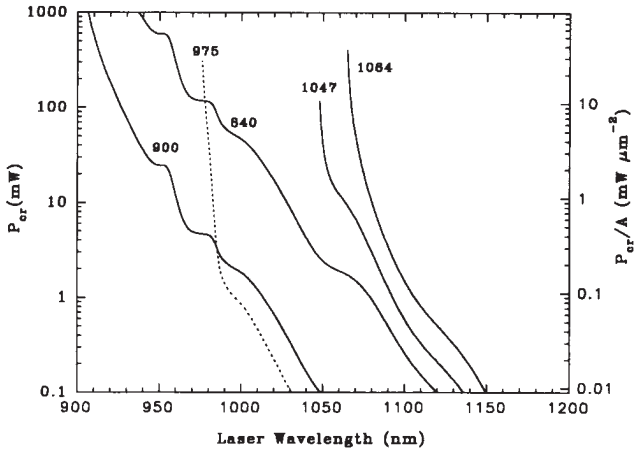

Fig. 2. Calculated values of the critical pump powers (for a 3.75μm diameter fiber) and intensities required to produce net gain (i.e., to reach transparency for the signal wavelength) in Yb^{3+}-doped silica fiber, plotted as a function of signal (lasing) wavelength and for various pump wavelengths.

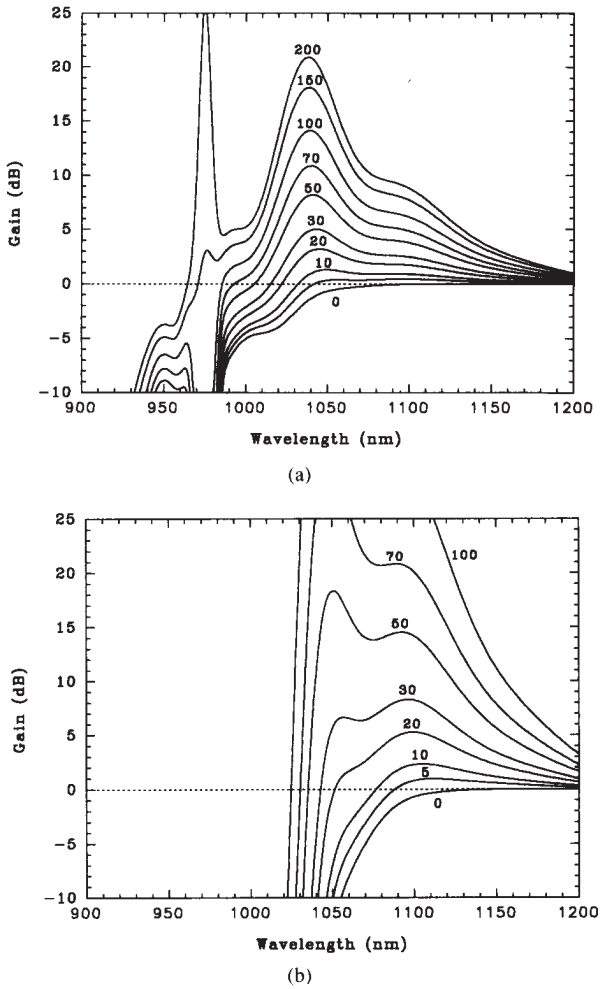

Fig. 3. Calculated gain spectrum for the specific case of pumping at 840 nm for two fiber lengths (a) 1m, (b) 20 m. (fiber diameter 3.75 μm, NA$\sim$0.17, [Yb^{3+}]$\sim$550 ppm). Curves are labeled with the launched pump power in milliwatts.

σ_{al}, the emission and absorption cross sections at the laser wavelength, and σ_{ep} and σ_{ap}, the emission and absorption cross sections at the pump wavelength, respectively. The critical power is independent of Yb^{3+} concentration, and whatever the fiber length or dopant concentration, for most efficient use of pump power, either at or above threshold, the power emerging from the fiber end (neglecting the Fresnel reflection) would, in fact, be equal to this critical power. Fig. 2 shows the critical power and also the corresponding intensities (for a typical fiber with diameter 3.75-μm) plotted as a function of lasing wavelength for various pump wavelengths of interest. This figure is useful in making design choices, as it can be seen that the critical powers are quite high for some combinations of pump and laser wavelengths. For example, to achieve lasing at 975 nm, it would be preferable to use a 900-nm pump source rather than an 840-nm pump source.

To further illustrate the dependence of lasing wavelength on pump conditions, we show the calculated gain spectrum for the specific case of pumping at 840 nm in Fig. 3(a). For low pump powers (5 mW) in the illustrated example, net gain first appears at long wavelengths $\sim$1100 nm for which there is negligible reabsorption from population in the lower level. Then, as pump power increases, the gain maximum moves progressively to shorter wavelengths, with the pure three level transition eventually having the dominant gain. The oscillation wavelengths under free-running conditions, i.e., without any wavelength selection applied, will correspond to the wavelength which has peak gain at the threshold for oscillation. With progressively harder pumping above threshold, assuming pure homogeneous broadening, the emission wavelength should remain clamped at its threshold value.

Some degree of control over the free-running wavelength can be achieved by changing the Q of the resonator, or by changing the fiber length. Changing the Q of the resonator changes the required gain for threshold, and therefore, the wavelength of peak gain, as can be seen in Fig. 3(a). Fig. 3(b) moved to longer wavelengths as a result of reabsorption in the extra length of fiber (e.g., compare the 30 mW curves in both figures). Thus oscillation at shorter wavelengths, e.g., at the 975 nm or 1040 nm gain peaks, can be suppressed by using a longer fiber to introduce reabsorption at these wavelengths. Alternatively one can use a longer pump wavelength (e.g., 1064 nm) than 975 nm or 1040 nm, thus ensuring no gain at these emission peaks. In this case a longer fiber is also needed, not to suppress the gain at 975 nm, but to ensure adequate absorption of the pump. While these two approaches both lead to the suppression of 975-nm gain, there is a difference which could become important under some circumstances. This is where short wavelength pumping is used and a very high gain at 975 nm is established at the input end of the fiber, although with net gain at 975 nm over the entire fiber length being suppressed by reabsorption further down the fiber. Under appropriate conditions strong ASE at 975 nm or even at $\sim$1040 nm could occur, and while the ASE travelling down the fiber would be reabsorbed and simply lead to a redistribution of

Data such as those presented in Fig. 3 are also useful in indicating the degree of frequency discrimination needed to enforce oscillation at wavelengths away from the free-running wavelength. Thus, from the data in Fig. 3(a) it is seen that to achieve oscillation at 1020 nm for a threshold pump power of 50 mW it is necessary to introduce ~5 dB of discrimination against 1040 nm to suppress its oscillation. Under higher gain conditions, i.e., for higher pump powers, the degree of frequency discrimination required can be seen to increase. As a general point, it should be noted that if the peak gain becomes high enough to allow strong ASE (~30-40 dB single-pass gain), then frequency discrimination via end reflectors, however great, will become ineffective. It is therefore clear that when oscillation in the low gain region of the emission spectrum is required (at long wavelengths or in the dip between the emission peaks) it is necessary to use a resonator having low loss at the desired oscillation wavelength. Fiber gratings are particularly well-suited to this need as they can provide both a high frequency discrimination and a very high reflectivity and, when written directly into the doped fiber, introduce negligible insertion loss. For example, with appropriate gratings we have achieved oscillation out to 1180 nm, and with further optimization and reduction of losses this could, in principle, be extended somewhat further.

This preceding discussion has indicated some of the main features that need to be considered when designing an Yb fiber laser to operate under specific conditions, particularly with regard to pump and operating wavelengths. It is seen that it is important to make appropriate choices of fiber length and concentration, resonator Q, and the degree of frequency discrimination. The next section provides an analytical treatment of Yb^{3+} fiber lasers, from which calculated data, such as in Fig. 3, are generated.

III. Calculation of Gain

For simplicity, we assume pump and laser intensity profiles to be uniform over the area A of the core and also assume a uniform dopant distribution within the core. Steady-state conditions are also assumed. The total populations of the $^2F_{7/2}$ and $^2F_{5/2}$ manifolds are designated N_1 and N_2, respectively. The total population N is then

$$N = N_1 + N_2. \tag{1}$$

Absorption $\sigma_a(\lambda)$ and emission $\sigma_e(\lambda)$ cross sections are defined such that the absorption coefficient at wavelength λ is $N_1\sigma_a(\lambda) - N_2\sigma_e(\lambda)$. For brevity we write $\sigma_a(\lambda_p)$ and $\sigma_e(\lambda_p)$ as σ_{ap} and σ_{ep} respectively, and $\sigma_a(\lambda_l)$ and $\sigma_e(\lambda_l)$ as σ_{al} and σ_{el}, respectively, where λ_p and λ_l are the pump and laser wavelengths, respectively.

The gain achieved in a length L is given by

$$\left(\frac{L}{l} \right)$$

where $g(z) = N_2(z)\sigma_{el} - N_1(z)\sigma_{al}$. The value of $N_2(z)$ and hence $N_1(z) = N - N_2(z)$, is determined from the pump power $P_p(z)$ at that location. $P_p(z)$ obeys the equation

$$\frac{dP_p(z)}{dz} = -N_1\,\sigma_{ap}\,P_p(z) + N_2\,\sigma_{ep}P_p(z). \tag{3}$$

Here we have assumed that background loss can be ignored. Our experimental results confirm that for fiber lengths up to ~100 m the background loss (estimated at < 10 dB/km) played a negligible role.

To solve for $P_p(z)$ we make use of (1) and of the relation

$$\frac{dP_p(z)}{dz} = -\frac{A\,h\,\nu_p}{\phi_p\,\tau}\,N_2(z) \tag{4}$$

where τ is the lifetime of the upper level and ϕ_p is the pumping quantum efficiency (in this case, for Yb^{3+}, $\phi_p \sim 1$).

From (1), (3), and (4) we obtain the result

$$\ln\left(\frac{P_p(z)}{P_p(0)}\right) + \frac{P_p(z) - P_p(0)}{P_s} = -N\sigma_{ap}z \tag{5}$$

where $P_p(0)$ is the input pump power and P_s is the pump saturation power (i.e., the power that reduces the absorption coefficient by a factor of 2).

P_s is given by

$$P_s = \frac{h\,\nu_p\,A}{(\sigma_{ep} + \sigma_{ap})\,\tau\,\phi_p}. \tag{6}$$

Thus, $P_p(z)$ can be calculated from (5).

The single-pass gain exponent (2) for a length l of fiber is then given by

$$(\sigma_{el} + \sigma_{al}) \int_0^l N_2(z)dz - N\sigma_{al}l$$

which can be reexpressed with the help of (4) as

$$\frac{\phi_p(\sigma_{el} + \sigma_{al})\tau P_a}{Ah\nu_p} - N\sigma_{al}l \tag{7}$$

where P_a is the absorbed power

$$P_a = P_p(0) - P_p(l). \tag{8}$$

Thus, the procedure for calculation of gain reduces to calculating $P_p(l)$ from (5), hence, P_a (via (8)), and then the gain exponent from (7), or expressed in dB

$$\text{gain} = 4.34\left[\frac{\phi_p(\sigma_{el} + \sigma_{al})\tau P_a}{Ah\nu_p} - N\sigma_{al}l\right]\text{dB}. \tag{9}$$

This expression simplifies if σ_{al} can be neglected, for example, for long wavelength operation, such as 1140 nm. Similarly, the expression for P_s is simplified when σ_{ep} is zero, as in the case where pumping is at short wavelengths, say less than 940 nm.

A generalization of the equations to deal with cladding-pumping is straightforward. If the area of the inner cladding into which the pump is launched is x times the area of the core,

becomes x times greater (6) and the right-hand side of (5) becomes $-N\sigma_{ap}z/x$.

The above analysis assumes that all the ions in the fiber are characterized by identical absorption and emission cross sections, i.e., that spectral broadening is homogeneous. The amorphous nature of a glass, however, leads to site-to-site variations of the local electric field, producing a degree of inhomogeneous broadening in the system. There is insufficient information available to accurately model the effect of any inhomogeneity. Spectral inhomogeneity could manifest itself in the form of spectral hole burning, either in pump absorption or laser emission. Since our analysis above is a small-signal analysis of the laser gain, however, the effects of spectral hole burning due to lasing can be neglected. They may, however need to be considered for operation above threshold.

IV. Spectroscopy

Successful modeling of the Yb^{3+} laser performance requires an accurate knowledge of the absorption and emission cross sections. The cross sections shown in Fig. 1(b) were determined experimentally, as described in this section.

The sidelight fluorescence spectrum was obtained, using an integrating sphere, from a length of fiber stripped of its protective jacket and pumped at 840 nm. The form of the emission cross section was determined by scaling the measured fluorescence spectrum by λ^5, and the absolute value of the emission cross section was then obtained by relating the integrated cross section to the measured upper level lifetime, using the relationship

$$W_{rad} = \frac{1}{\tau} = \frac{8\pi n^2}{c^2} \int \nu^2 \sigma_{em}(\nu)\, d\nu. \qquad (10)$$

The decay of sidelight fluorescence from $^2F_{5/2}$ was measured by chopping the pump acoustooptically at ~60Hz. The fluorescence was collected by a bundle of fibers and imaged onto a silicon photodiode. The fluorescence decayed exponentially over the first three e-folds, with a decay time of ~840 μ's. The energy spacing between the two manifolds (>10 000 cm^{-1}) greatly exceeds the maximum phonon energy in silica (~1100 cm^{-1}), and the observed fluorescence lifetime is taken to be the radiative lifetime.

The form of the absorption cross section was measured from the transmission of a white light source using a cut back technique. The well resolved peak at 975 nm that appears both in emission and absorption corresponds to transitions between the lowest energy Kramers doublets in the ground and excited manifolds. The absorption spectrum was scaled to give equal absorption and emission cross sections at the peak wavelength. This is an approximation, because the crystal field splitting is larger in the excited manifold than in the ground manifold and the degeneracy is lower; a McCumber analysis suggests that at room temperature the absorption cross section may be 5–10% larger than the emission cross section. This discrepancy is comparable with other experimental uncertainties. The profiles of the room temperature absorption and emission cross section parameter ϵ was taken to be the energy difference corresponding to the sharp peaks (at 975 nm) in the absorption and emission spectra. An independent confirmation of this scaling was obtained from a measurement of fluorescence sidelight as a function of pump power. The pump power (at 1017 nm) required to reach half the maximum fluorescence intensity (pump saturation power) is given by (6). This measurement gave a value for $(\sigma_a + \sigma_e)$ of 0.43±0.1 pm^2, in fair agreement with the value obtained from the absorption and emission cross sections (0.39 pm^2). This result justifies the assumption that the $^2F_{5/2}$ lifetime is predominantly radiative.

To determine the concentration of Yb^{3+} in the fibers used, cutback measurements were performed using low incident powers. Assuming a Beer's law distribution of pump power along the fiber, the small-signal absorption coefficient was deduced which is the product of the dopant concentration, cross section, and overlap integral of the pump with the dopant. The overlap integral is not easily calculated; the distribution of the dopant across the fiber core tends to follow the germania distribution and varies with fiber drawing conditions. Therefore, we have chosen to work with an effective concentration, i.e., the product of the concentration and overlap integral. The effective concentration estimated in this way is 550±100 ppm.

V. Operation as a Free-Running Laser

In this section, the operating characteristics of single-spatial-mode, free-running Yb^{3+} lasers are presented. The results have been chosen to illustrate the versatility and general principles of laser action in Yb^{3+}-doped silica fibers and to show the agreement between theory and experiment. The Yb^{3+}-doped germanosilicate fibers used for these experiments had numerical aperture ~0.17, and dopant concentration ~550 ppm, and diameters of either 3 μm or 3.75 μm. The background loss was found to be < 10 dB/km. Pump light, from either a Ti-sapphire laser, Nd:YLF or Nd:YAG laser was launched into the fiber using a x10 or x16 microscope objective, and laser action was investigated for resonators with feedback provided by two bare, cleaved fiber ends, or one cleaved end and a butted dielectric-coated mirror at the other end. Typical launch efficiencies varied from ~50% for the Ti-sapphire laser to ~70% for the Nd:YLF laser.

Laser action has been investigated for pumping at wavelengths from 840–1064 nm. In all cases, very efficient laser operation can be achieved, with slope efficiencies of up to 90% with respect to absorbed power. Depending on the fiber length and optical feedback, laser operation has been demonstrated from 1035–1115 nm.

In Fig. 4, the results of modeling calculations (line) are compared with measurements (symbols) of threshold powers and lasing wavelength as a function of fiber length. Threshold powers (Fig. 4(a)) are in terms of launched pump power, and the calculated thresholds are seen to be within 30% of the measured thresholds. The trends predicted by the modeling are confirmed by the experimental measurements.

There is clearly an optimum length for reaching threshold for laser action at low values of launched pump powers,

DOCKET ALARM

Explore Litigation Insights

Docket Alarm provides insights to develop a more informed litigation strategy and the peace of mind of knowing you're on top of things.

Real-Time Litigation Alerts

Keep your litigation team up-to-date with **real-time alerts** and advanced team management tools built for the enterprise, all while greatly reducing PACER spend.

Our comprehensive service means we can handle Federal, State, and Administrative courts across the country.

Advanced Docket Research

With over 230 million records, Docket Alarm's cloud-native docket research platform finds what other services can't. Coverage includes Federal, State, plus PTAB, TTAB, ITC and NLRB decisions, all in one place.

Identify arguments that have been successful in the past with full text, pinpoint searching. Link to case law cited within any court document via Fastcase.

Analytics At Your Fingertips

Learn what happened the last time a particular judge, opposing counsel or company faced cases similar to yours.

Advanced out-of-the-box PTAB and TTAB analytics are always at your fingertips.

API

Docket Alarm offers a powerful API (application programming interface) to developers that want to integrate case filings into their apps.

LAW FIRMS
Build custom dashboards for your attorneys and clients with live data direct from the court.

Automate many repetitive legal tasks like conflict checks, document management, and marketing.

FINANCIAL INSTITUTIONS
Litigation and bankruptcy checks for companies and debtors.

E-DISCOVERY AND LEGAL VENDORS
Sync your system to PACER to automate legal marketing.